



Original Article

## Elucidating the unintentional p-type nature of spinel $\text{Co}_3\text{O}_4$ : A defect study using ab-initio calculation



Sung Beom Cho, Eun Seob Sim, Yong-Chae Chung\*

Division of Materials Science and Engineering, Hanyang University, 222 Wangsimni-ro, Seongdong-gu, Seoul, 04763, Republic of Korea

### ARTICLE INFO

**Keywords:**  
Intrinsic doping  
Spinel oxide  
Ab-initio thermodynamics

### ABSTRACT

$\text{Co}_3\text{O}_4$  is one of the most widely used materials in energy and environmental field due to its unintentional p-type nature, which depends on the preparation conditions. In this study, we investigated the origin of the unintentional p-type conductivity of  $\text{Co}_3\text{O}_4$  by calculating all possible intrinsic point defects. We found that the octahedral cobalt vacancy and tetrahedral cobalt vacancy are the sources of unintentional p-type doping. Using charge balance theory, we analyzed the effect of preparation condition on intrinsic defect-induced doping. In most of preparation condition, the formation of these cobalt vacancies plays a dominant role and the spontaneous formation of p-type doping is unavoidable. However, if there is ample oxygen and the temperature is low during the preparation, the unintentional p-type doping can be avoided. This theoretical work on defects provides a crucial clue to optimize  $\text{Co}_3\text{O}_4$  for various electrochemical applications.

### 1. Introduction

$\text{Co}_3\text{O}_4$  is an important technological materials in the energy and environmental field, due to its low cost and low environmental footprint [1–3]. Recently,  $\text{Co}_3\text{O}_4$  has emerged as one of the most promising materials in electrochemical applications such as Li-ion battery electrodes [4–6], supercapacitor electrodes [7–9], and electrocatalysts [10–12]. The use of  $\text{Co}_3\text{O}_4$  is attractive because it can enhance the performance of electrochemical devices due to a combination of its two excellent materials property. One is chemical reactivity and the other is electrical conductivity. The chemical reactivity of  $\text{Co}_3\text{O}_4$  has been intensively investigated experimentally and by simulations at the atomic-scale [13–15]. These studies on  $\text{Co}_3\text{O}_4$  guided efforts to optimize the surface structure to improve its catalytic performance. However, the electrical properties of  $\text{Co}_3\text{O}_4$  are still not fully understood at the atomic-scale even though it is another crucial criteria for electrocatalytic materials. Though its electrical property is known as p-type semiconductor by thermoelectric power measurement on  $\text{Co}_3\text{O}_4$  [16], the origin of this semiconductivity is still unclear. Some have suggested that the p-type conductivity is due to the point defects in  $\text{Co}_3\text{O}_4$ , but the type of defect and the relation with the preparation conditions are still unclear [17]. This lack of understanding limits the optimization of the material properties for energy and environmental applications.

$\text{Co}_3\text{O}_4$  can be prepared using various methods, such as CoO oxidation [18], chemical vapor deposition [16,19,20], and hydrosynthesis [21]. These preparation methods should include crystal growth, which

induces the agglomeration of nanocrystals during the nucleation and growth process. Defect formation is unavoidable even in nanoparticles due to the agglomeration [22,23]. Furthermore, the species and concentration of the defects highly depend on the preparation conditions. We expect that the various defects can be formed in the preparation of  $\text{Co}_3\text{O}_4$ , and the species and concentration of the defects should depend on the preparation conditions [24]. Recent studies of  $\text{Co}_3\text{O}_4$  electrodes have reported that the electric and electrocatalytic properties of  $\text{Co}_3\text{O}_4$  can be widely tuned by changing the preparation conditions [25]. Understanding how  $\text{Co}_3\text{O}_4$  preparation conditions influence, the point defect can provide a crucial clue to understanding the wide variation of material properties in  $\text{Co}_3\text{O}_4$ .

In this study, we investigated the point defects of  $\text{Co}_3\text{O}_4$  using Density Functional Theory (DFT) calculations. All possible point defects was calculated considering the preparation conditions under O-rich, intermediate, and Co-rich environments. We also studied how the contribution of the point defects influenced the conductivity.

### 2. Calculation details

#### 2.1. DFT calculations

DFT calculations were performed using a projector augmented wave (PAW) pseudopotential [26] method as implemented in the Vienna Ab-initio Simulation Package (VASP) [27]. The plane wave basis set and periodic boundary condition were adopted to solve the Kohn-Sham

\* Corresponding author.

E-mail address: [yongchae@hanyang.ac.kr](mailto:yongchae@hanyang.ac.kr) (Y.-C. Chung).

equation. The exchange correlation interaction was described with the Perdew, Burke, and Ernzerhof (PBE) potentials [28]. In our all PAW calculations, the  $3s^23p^63d^74s^2$  electrons of cobalt and the  $2s^22p^4$  electrons of oxygen were treated as valence electrons. Furthermore, on-site correction for the Coulomb ( $U$ ) and exchange ( $J$ ) interactions of d-electrons (DFT +  $U$ ) was applied to consider the effect of 3d electron correlation. Dudarev's invariant approach [29] was adopted for the DFT +  $U$  calculation, and the on-site exchange interaction parameter  $J$  was set to its typical value of 1 eV [30]. Herein, effective  $U-J$  of 3 eV was used to correct the bandgap.

The magnetic moment of  $\text{Co}_{\text{g}}^{2+}$  ion is  $2.54\mu_B$ , whereas  $\text{Co}_{\text{l6d}}^{3+}$  is not magnetic. The experimental value of  $\text{Co}^{2+}$  is  $3.02\mu_B$ . This underestimation is due to difficulty in partitioning the electron distribution to a specific atom in the solid and to the self-interaction error of the exchange-correlation functionals [14,31]. To produce a more accurate magnetic moment, two different  $U_{\text{eff}}$  values for  $\text{Co}^{2+}$  and  $\text{Co}^{3+}$  can be employed [32]. However, for the defect calculations, it is difficult to pre-identify the oxidation state of the involved ions when the additional charged interstitial ions or vacancies are generated. The use of multiple  $U$  values is not appropriate for determining the formation energy in this case. Therefore, a single  $U$  value model is adopted for surface calculations involving  $\text{Co}_3\text{O}_4$  [33].

All atomic structures were fully relaxed until the maximum total Hellmann-Feynmann force was less than  $0.02 \text{ eV}/\text{\AA}$  and a total energy convergence within  $10^{-5} \text{ eV}$  was achieved. The normal spinel  $\text{Co}_3\text{O}_4$  was treated as a conventional cubic unit cell, which was composed of 56 atoms as shown in Fig. 1a. The initial  $k$ -point integration was carefully determined with at least 35  $k$  points irreducible in the first Brillouin zone after the convergence test [34]. The cutoff energy for the plane wave expansion was set to be 700 eV for more precise lattice relaxation. The calculated lattice parameter was  $8.134 \text{ \AA}$ , which is reasonably consistent with the experimental value of  $8.08 \text{ \AA}$  [35,36].

## 2.2. Charged defect calculation

The charged point defects were described using a periodically repeated supercell model. However, the supercell approach can introduce artifacts while estimating the total energy [37]. To avoid artifacts while evaluating the total energy of the supercell containing charged defects, two types of correction schemes were applied in all charged defects calculations. Of course, this correction term is equal to zero in the neutral supercell. The first term is a correction for the shift of the average electrostatic potential with respect to the bulk. Since the term for the average electrostatic potential in the supercell is conventionally determined as zero under the pseudopotential momentum-space method [38], the eigenvalues of the cell are shifted to an arbitrary constant. This error was corrected by calculating the difference between

the average electrostatic potential in a bulk-like environment of the defective supercell and the average electrostatic potential in the defect-free supercell. The other error came from the interaction between the charged defects and their periodic images. This effect was corrected by the Makov-Payne method [39], which describes electrostatic interaction energy between the point charge and its Madelung-like lattice energy of the point charge. The correction term is expressed as

$$E_{\text{cor}} = -\frac{q^2\alpha}{4\pi L\kappa\epsilon_0} \quad (1)$$

where  $q$  is the charge on the defect,  $\alpha$  is the Madelung constant,  $L$  is the length of the cubic supercell used for calculations, and  $\kappa$  is the dielectric constant of  $\text{Co}_3\text{O}_4$ . A dielectric constant of 12.9 was used [19] and the typical correction was on the order of  $0.05q^2 \text{ eV}$ .

The formation energies of the charged defect were calculated using the thermodynamic formalism with the chemical potential of the reservoir of elements and electrons [40,41]. Within the supercell model, the formation energy of the charged defect was evaluated by

$$\Delta H_f(D^q, \mu, \epsilon_F) = (E^{D^q} - E^{\text{Bulk}}) + \sum_i n_i(\mu_i^0 + \Delta\mu_i) + q(\epsilon_F + \epsilon_{\text{VBM}}) \quad (2)$$

where  $E^{D^q}$  is the energy of the supercell containing a defect in a charge state of  $q$ , and  $E^{\text{Bulk}}$  is the energy of the defect-free supercell. The second term represents the atomic reservoir of element  $i$  removed ( $n_i = +1$ ) or added ( $n_i = -1$ ) to the supercell when the defect is formed. This term is described based on reference state of species  $\mu_i^0$  and chemical potential  $\Delta\mu_i$ . The third term represents the reservoir for the electrons in the charged state, which ranges from the valence band maximum (VBM) to the conduction band minimum (CBM). This term is described with the parametric Fermi level ( $\epsilon_F$ ) which is referenced to the VBM and the eigenvalue of VBM ( $\epsilon_{\text{VBM}}$ ).

The chemical potential of cobalt and oxygen depends on the preparation condition but constraints exist during the formation of the  $\text{Co}_3\text{O}_4$  crystal. The constraint is given by

$$3\Delta\mu_{\text{Co}} + 4\Delta\mu_{\text{O}} = \Delta H_f(\text{Co}_3\text{O}_4) \quad (3)$$

where  $\Delta H_f(\text{Co}_3\text{O}_4)$  is the formation enthalpy of the  $\text{Co}_3\text{O}_4$  crystal. The formation enthalpy of the  $\text{Co}_3\text{O}_4$  was calculated with the total energy of bulk cobalt oxide,  $E(\text{Co}_3\text{O}_4)$ , and standard states of each element, bulk cobalt crystal and oxygen molecules, as follows.

$$\Delta H_f(\text{Co}_3\text{O}_4) = E(\text{Co}_3\text{O}_4) - 3E(\text{Co}) - \frac{1}{2}E(\text{O}_2) \quad (4)$$

Herein, the calculated formation energy was  $-9.71 \text{ eV}$ , and the experimental value was  $-9.43 \text{ eV}$  [42]. Within the constraint, we considered three representative preparation conditions. One is the O-rich condition, which is  $\Delta\mu_{\text{O}}$  is governed by the reference state,  $\text{O}_2$ . In this condition, the chemical potential of each element is defined by

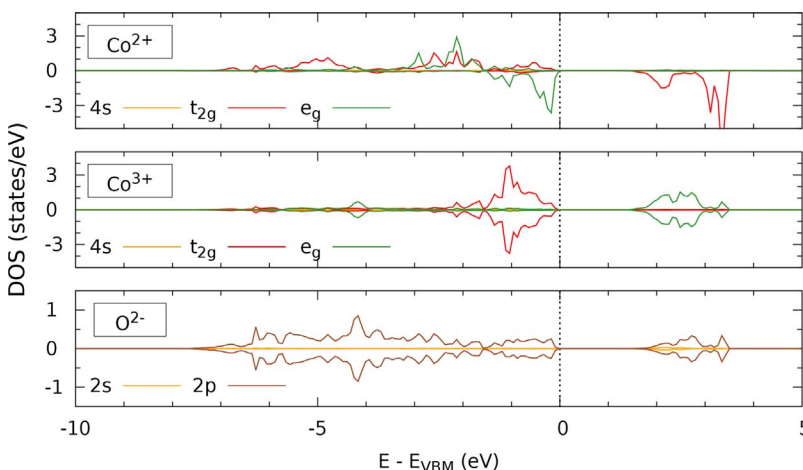


Fig. 1. Atomic orbital projected density of state of bulk  $\text{Co}_3\text{O}_4$ .

$\Delta\mu_O = 0$ ;  $\Delta\mu_{Co} = \frac{1}{3}\Delta H_f(Co_3O_4)$ . Similarly, The Co-rich condition is characterized by  $\Delta\mu_{Co} = 0$ ;  $\Delta\mu_O = \frac{1}{4}\Delta H_f(Co_3O_4)$ . To consider more general cases, we also considered the intermediate condition of  $3\Delta\mu_{Co} = 4\Delta\mu_{ceO} = \frac{1}{2}\Delta H_f(Co_3O_4)$ . We also determined that CoO was not formed as a secondary phase in the defined range of the chemical potentials (please see supplemental materials).

The thermodynamic transition levels between charge states  $q$  and  $q'$  in a defect are defined as

$$\epsilon_D \left( \frac{q}{q'} \right) = \frac{\Delta H_f(D, q) - \Delta H_f(D, q')}{q' - q} \quad (5)$$

This equation is obtained by comparing Eq. (2) in the charge state of  $q$  and  $q'$ . The term  $\epsilon_D(q/q')$  represents the energy level where the charge state is changed from  $q$  to  $q'$ . The optical transition level induced by the defects is also calculated from the energetics of the charged states and related atomic coordinates [40]. This is because the optical transition level can be divided into two steps. One step is for the change in the charged state of defects that is directly related to light absorption or emission. The other step is for atomic relaxation after the change in charge state. Therefore, we can calculate the energetics of each step by manipulating the charge state and atomic coordinates. The energy of the light absorption or emission was calculated based on the energy difference between two different charged states with fixed the atomic coordinates. The energy of the lattice relaxation was obtained by the energy difference between two atomic coordinates with the same charge states.

### 2.2.1. Charge balance equation

If there are no external variables, the concentration of the defects depends on the formation energy. When defects are formed, extra carriers such as excited electrons and holes can be generated. In this situation, the generation of defects and extra carriers should meet the charge neutrality condition to maintain the stability of  $Co_3O_4$  as follows:

$$n - p = \sum_D q c(D, q), \quad (6)$$

where,  $n$  and  $p$  are the concentration of the excited electrons and holes, respectively, and  $c(D, q)$  is the concentration of defect species  $D$  with charge  $q$ . The left terms of the equation,  $n$  and  $p$ , are given by the Fermi-Dirac distribution function,  $f(\epsilon, T, E_F)$ , and the density of states of  $Co_3O_4$ ,  $n(\epsilon)$ , as follows:

$$n = \int_{\epsilon_{CBM}}^{\infty} n(\epsilon) f(\epsilon, T, E_F) d\epsilon,$$

$$p = \int_{-\infty}^{\epsilon_{VBM}} n(\epsilon) f(\epsilon, T, E_F) d\epsilon.$$

The evaluation of  $n$  and  $p$  requires a very accurate estimation of  $n(\epsilon)$ , but it can be simplified in the dilute limit as follows:

$$n = N_{CBM} \exp \left( -\frac{\epsilon_{CBM} - \epsilon_F}{kT} \right),$$

$$p = N_{VBM} \exp \left( -\frac{\epsilon_F - \epsilon_{VBM}}{kT} \right),$$

where  $k$  is the Boltzmann constants,  $T$  is temperature, and  $N_{CBM}$  and  $N_{VBM}$  are effective densities of states in the conduction and valence bands, respectively. The effective density of states can be described using the effective mass of electrons ( $m_e$ ) and holes( $m_h$ ) at temperature  $T$ ,

$$N_{CBM} = 2 \left( \frac{m_e k T}{2\pi \hbar^2} \right)^{3/2},$$

$$N_{VBM} = 2 \left( \frac{m_h k T}{2\pi \hbar^2} \right)^{3/2}.$$

The effective mass is evaluated using a parabolic approximation,

$$\epsilon(\mathbf{k}) = \epsilon_0 + \frac{\hbar^2 \mathbf{k}^2}{2m^*}. \quad (7)$$

The left side of the equaiton,  $n - p$ , can be expressed as a function of  $\epsilon_F$  and  $T$ . The right side of the equation,  $c(D, q)$  can also be a function of  $\epsilon_F$  and  $T$  considering it follows a Boltzmann distribution,

$$c(D, q) = \exp \left( -\frac{\Delta H_f(D, \mu, \epsilon_F)}{kT} \right). \quad (8)$$

The defect formation energy  $\Delta H_f(D, \mu, \epsilon_F)$  is a function of  $\epsilon_F$  for given defect species and synthesis environments; therefore, the right term of the charge neutrality equation is a function of  $\epsilon_F$  and  $T$ . Thus, we evaluated the Fermi energy,  $E_F$  of a given system, by numerically solving  $\epsilon_F$  in this equation for given  $T$ .

## 3. Results and discussion

### 3.1. Defect-free structure of $Co_3O_4$

The direct bandgap calculated using Dudarev's method was 1.503 eV. This result is in good agreement with experimental observations of the direct optical transition at 1.44–1.52 eV [43,44]. The VBM and CBM of  $Co_3O_4$  are composed of d orbital of Co and p orbital of O ions. The orbital projected density of states are shown in Fig. 1. The  $e_g$  state of  $Co^{2+}$  and the  $t_{2g}$  state of  $Co^{3+}$  constitute the VBM, while the  $t_{2g}$  state of  $Co^{2+}$  and  $e_g$  state of  $Co^{3+}$  constitute the CBM. Otherwise, the  $4s$  state of both the cobalt ions vanishes because of charge transfer to the  $2p$  orbitals. The transferred electrons are accumulated in the  $2p$  orbitals of oxygen ions and form the VBM. However, the  $2p$  state of oxygen still remains at the CBM. This lack of change is because the conduction band is made up of a hybridization between the d orbital of Co and the  $2p$  orbitals.

### 3.2. Defect of $Co_3O_4$

The structure of spinel cobalt oxide is based on a face centered cubic (FCC) array of oxygen ions, where cobalt ions occupy 8a tetrahedral interstices ( $Co^{2+}$ ) and 16d octahedral interstices ( $Co^{3+}$ ), as shown in Fig. 2. Based on the spinel structure, we calculated all possible native defects including oxygen vacancy ( $V_{O(32e)}$ ), tetrahedral cobalt vacancy ( $V_{Co(8a)}$ ), octahedral cobalt vacancy ( $V_{Co(16d)}$ ), tetrahedral cobalt interstitial ( $Co_{i(48f)}$ ), octahedral cobalt interstitial ( $Co_{i(16c)}$ ), tetrahedral oxygen interstitial( $O_{i(48f)}$ ), and octahedral oxygen interstitial( $O_{i(16c)}$ ). All of the charge states of the defects were considered under the O-rich, intermediate, and Co-rich preparation conditions. The formation energies for the defects in the most stable charge state are calculated as function of parametric Fermi level,  $\epsilon_F$ , as shown in Fig. 3.

The  $\epsilon_F$  represents the energy of electron reservoir at the formation of defect, not Fermi level determined by intrinsic doping (discussed later). This  $\epsilon_F$  can be varied by synthetic constraint, for instance, electric gating, interface pinning by substrate, heavy doping by impurity. The slope in Fig. 3 represents the charge state of the defects, and the kinks indicate a transition between the charge states. The transition level and the stable charge state of the defects within the bandgap are shown in Fig. 4.

### 3.3. O-rich condition

Under O-rich conditions, the chemical potential of oxygen is high, and the chemical potential of the cobalt is low. The defect formation energy under the O-rich conditions is plotted in Fig. 3a. For  $\epsilon_F$  near the CBM,  $O_{i(48f)}$  is the most stable defect. However, it is not expected to be the dominant defect due to its high formation energy. On the other hand, for the  $\epsilon_F$  near the VBM,  $V_{Co(16d)}$  is the dominant defect. The 16d site is for octahedral  $Co^{3+}$  ions, which do not have a magnetic moment. Our determination of the dominant defect is consistent with the experimental result of Angelov et al. [45]. In their experiments, they compared the EPR signals of stoichiometric  $Co_3O_4$ , O-rich  $Co_3O_4$ , and

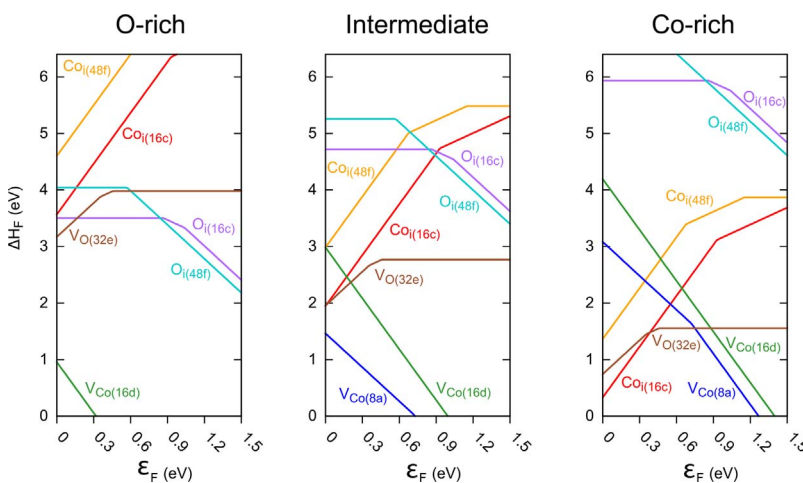
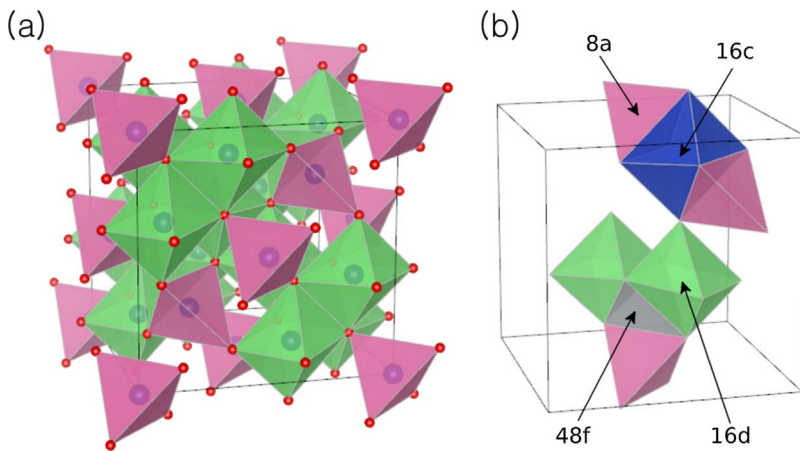
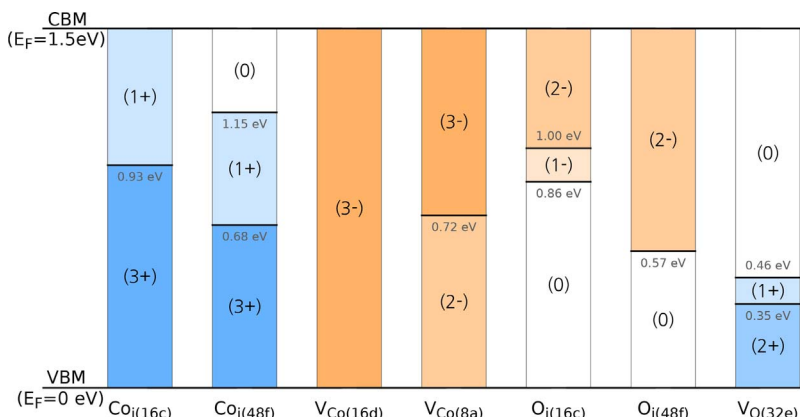


**Fig. 3.** Formation energy of defects as function of energy of electron reservoir ( $\epsilon_F$ ) under O-rich condition, intermediate condition, and Co-rich condition.



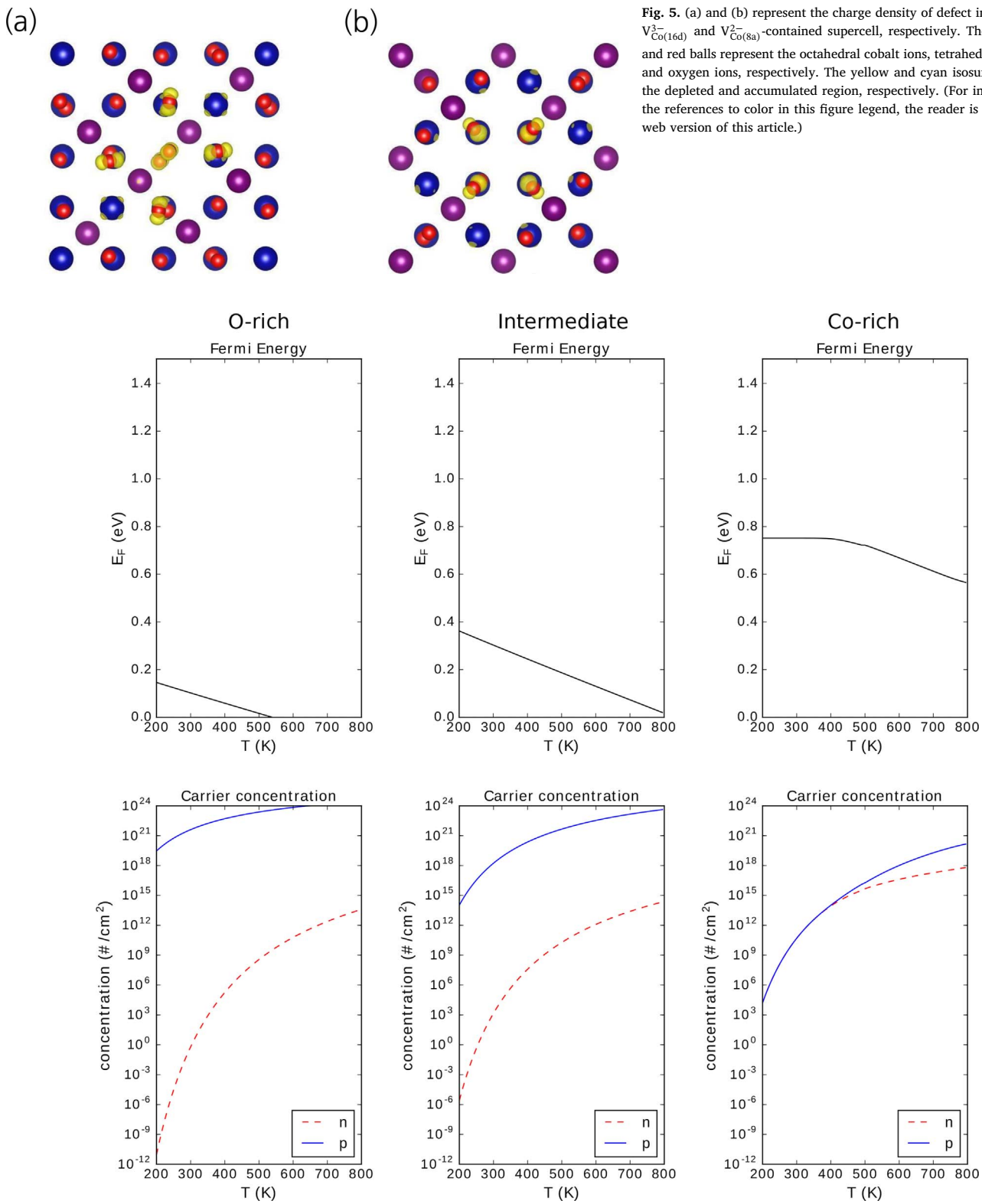
Li-doped O-rich  $\text{Co}_3\text{O}_4$ . They proposed that the defects created in O-rich condition are octahedral vacancies based on a comparison of the exchange interaction between tetrahedron  $\text{Co}^{2+}$  ions of these samples. This experimental result is in good agreement with our computational results that the dominant defect,  $\text{V}_{\text{Co}(16\text{d})}^{3-}$ , does not change the magnetic moment near  $\text{Co}^{2+}$ .

According to our calculations, the octahedral cobalt vacancies,  $\text{V}_{\text{Co}(16\text{d})}$ , showed as 3<sup>-</sup> of the charge state. This result implies that  $\text{V}_{\text{Co}(16\text{d})}$  can be a source of p-type conductivity because the defect shallows the electron generating the hole. This charge state is related to the neighboring oxygen. Six undercoordinated oxygen ions are generated when the neutral octahedral cobalt vacancy is formed. These undercoordinated oxygen ions have unfilled 2p orbitals with a mainly

VBM character. Most defect-induced states are spatially localized on these undercoordinated oxygen ions, as shown in Fig. 5a.

The atomic charge population of the undercoordinated oxygen ions is restored to that of the oxygen ions in defect-free supercells within 0.02e. The  $\text{V}_{\text{Co}(16\text{d})}^{3-}$  increases the edge length of the octahedron by 15% and induces 2% tensile strain. The electron fully occupies the defect level of the 2p orbital, and this occupied state is more stable than the partially occupied state.

The formation of octahedral cobalt vacancies,  $\text{V}_{\text{Co}(16\text{d})}$ , triggers p-type doping. Fig. 6 shows the calculated Fermi level and carrier concentration during the synthesis process. The Fermi level under O-rich conditions ranged from 0 eV to 0.15 eV, and  $\text{V}_{\text{Co}(16\text{d})}$  can easily form. Because  $\text{V}_{\text{Co}(16\text{d})}$  can serve as an acceptor, the concentration of the holes

Fig. 6. Equilibrium position of the Fermi level,  $\epsilon_F$ , for synthesis condition.

is much higher than that of electrons. Therefore, the  $\text{Co}_3\text{O}_4$  is spontaneously p-type doped due to its intrinsic defect,  $\text{V}_{\text{Co}(16d)}$ . As the temperature increases, the Fermi level decreases, and more holes are generated. Therefore, the electrical conductivity of  $\text{Co}_3\text{O}_4$  can be enhanced by synthesis at high temperature. The Fermi level decreases until 537 K, where the value is zero. If the temperature is higher than 537 K, there is no solution in the bandgap region. This means that the preparation

condition is out of our dilute limit approximation, and the stability may be compromised.

### 3.4. Intermediate conditions

Intermediate conditions are expected to be the most widely adopted to prepare  $\text{Co}_3\text{O}_4$ . The chemical potential of cobalt is similar to that of

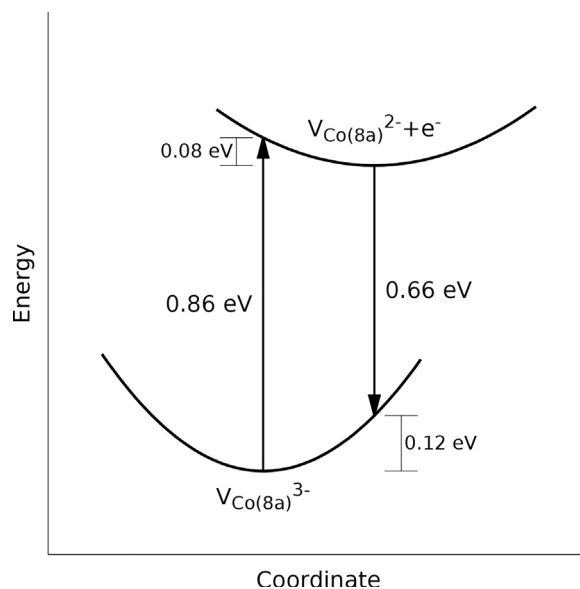


Fig. 7. Schematic configuration coordinate diagram for optical transition due to  $V_{Co(8a)}$ .

oxygen. Under this condition, the formation energy of the defect is plotted in Fig. 3. For a Fermi-level near the CBM,  $V_{O(32e)}$  is the most stable defect but it cannot be a dominant defect. It has high formation energy and shows a deep level property near the CBM. On the other hand,  $V_{Co(8a)}$  is expected to play a dominant role for a Fermi-level near the VBM. This vacancy is a shallow defect near the VBM, and its stable charge state is 2<sup>-</sup> at this level. This implies that  $V_{Co(8a)}$  can be a source of p-type conductivity.

The  $V_{Co(8a)}$  is formed by removing the tetrahedral  $Co^{2+}$  ions. When a neutral  $V_{Co(8a)}$  is generated, four undercoordinated oxygen ions are generated. Near the VBM, the 2-state is stable, and it occupies the unfilled 2p orbitals of the undercoordinated oxygen ions, as shown in Fig. 5b. The atomic charge population of the undercoordinated oxygen ions is restored to that of the oxygen ions in a defect-free supercell within 0.01e. The edge length of the tetrahedron increased by 5% due to the  $V_{Co(8a)}^{2-}$ . The lattice parameter of the supercell also increased by 1%. The spin redistribution induced by this defect is not remarkable. The induced change in the magnetic moment on one tetrahedral cobalt is within 0.02  $\mu_B$ . This is because the spin interaction between tetrahedral cobalt ions is weak enough to allow a paramagnetic phase with a Néel temperature of 40 K [32]. On the other hand, as shown in Fig. 5, the 3-state can also be a stable charge state as the Fermi level reaches the CBM. Because the two electrons are almost sufficient to fill the defect states, the extra electron exhibits behavior characteristic of the CBM in the Co-O covalent bond.

Because both charge states can exist at the transition level, this transition level can play a role as an acceptor level associated with the optical level. The thermodynamic transition of the charge state occurs at 0.72 eV, and the expected optical transition is shown in Fig. 7.

Due to the electron-hole pair from the excitation, the  $V_{Co(8a)}^{3-}$  turned into  $V_{Co(8a)}^{2-}$ . Recombination of an electron in the CBM with  $V_{Co(8a)}^{2-}$  leads to an emissions of 0.66 eV. The calculated emission level of 0.66 eV matches the recently observed narrow peak of  $Co_3O_4$ . Recently, Qiao et al. observed a bandgap of 0.74 eV from the photoluminescence properties [46]. The origin of the narrow peak was not determined, so the influence of defects cannot be ruled out. Considering the limitation of the exchange correlation function in this calculation, the calculated defects could provide a crucial clue to explain the narrow peak.

Under intermediate preparation conditions, both cobalt vacancies,  $V_{Co(8a)}$  and  $V_{Co(16d)}$ , play dominant roles for doping. As shown in Fig. 6, hole generation is much more likely than the electron generation, and the Fermi level is determined near the VBM, i.e., the bottom region of

the bandgap. This means that  $Co_3O_4$  is p-type doped under intermediate conditions due to intrinsic defects. However, the doping rate is much weaker than that under O-rich preparation condition. This is because the formation energies of cobalt defects are higher than those in O-rich condition. Therefore, spontaneous p-type doping is unavoidable for preparation under the intermediate conditions and under the O-rich condition.

### 3.4.1. Co-rich conditions

Co-rich conditions represent a state where the chemical potential of cobalt is high. Under these conditions, various defects can be found. Near the CBM,  $V_{Co(16d)}$  and  $V_{Co(8a)}$  were found to be the dominant defects. These cobalt vacancies are acceptors.  $Co_{i(16c)}$  and  $V_{O(32e)}$  were found to be dominant defects, for the Fermi level near the VBM. The  $Co_{i(16c)}$  showed 3<sup>+</sup> charge state, which shows typical negative-U behavior due to a decrease in the cell volume by 7.5 Å<sup>3</sup> [47]. The charge state of the  $V_{O(32e)}$  is 2<sup>+</sup>, 1<sup>+</sup>, or 0 depending on the position of the Fermi level. Both  $Co_{i(16c)}$  and  $V_{O(32e)}$  can serve as donor. Likewise, various defects can be generated under Co-rich condition.

Fig. 6 shows how the defects contribute to the electrical properties. In the low temperature region, surprisingly, the Fermi-level is in the center of the bandgap, as in an intrinsic semiconductor. This is because any of defects cannot play a significant role, but they compensate for each other as donors or acceptors. Therefore, unintentional p-type doping is not observed in this condition. However, as the temperature increases, the role of the cobalt vacancies becomes dominant. More holes are generated and the  $Co_3O_4$  becomes p-type doped. However, due to compensation by donors like  $Co_{i(16c)}$  and  $V_{O(32e)}$ , the increase in doping rate is much slower than in the other preparation conditions.

## 4. Conclusion

In this study, all possible charge states of intrinsic point defects of  $Co_3O_4$  were investigated using a DFT + U approach. All representative preparation conditions were considered. Combining ab-initio thermodynamic techniques, the dominant point defect was determined under O-rich, intermediate, and Co-rich preparation conditions, and their effects on spontaneous doping was investigated. The DFT calculation provides crucial clues to explain the unintentional p-type conductivity of  $Co_3O_4$ , which is a fundamental electrochemical property. The results of the intrinsic defects indicate that the cobalt vacancies are the origin of the p-type conductivity. The octahedral cobalt vacancy,  $V_{Co(16d)}$ , was found to be the dominant defect under O-rich conditions. This dominant defect,  $V_{Co(16d)}$ , is a shallow acceptor, making it a source of p-type conductivity. The dominance of  $V_{Co(16d)}$  produces heavily doped  $Co_3O_4$  and can damage the material under high temperature. Under intermediate condition, both of the octahedral cobalt vacancy,  $V_{Co(16d)}$ , and the tetrahedral cobalt vacancy,  $V_{Co(8a)}$ , can also be a dominant defect and a source of p-type conductivity. The charge transition level of the  $V_{Co(8a)}$  is expected to induce an optical transition, which is experimentally observable. The preparation of  $Co_3O_4$  under intermediate condition cannot avoid unintentional p-type doping due to the contribution of those two defect. On the other hand, unintentional p-type doping by native point defects can be avoided in Co-rich conditions. Under low temperature, various defects are generated and they compensate for each other. In this case, the  $Co_3O_4$  behaves like an intrinsic semiconductor. However, if the temperature increases, more holes are generated than electrons, resulting in a p-type material. This implies that unintentional doping can be avoided under Co-rich conditions by controlling the temperature. This study of the dominant defect and their charge states provides a guide to enhance or avoid the p-type conductivity of  $Co_3O_4$ .

## Acknowledgements

This research was supported by Basic Science Research Program

through the National Research Foundation of Korea (NRF) funded by the Ministry of Science, ICT and Future Planning (2016R1A2B4010674).

## Appendix A. Supplementary data

Supplementary data associated with this article can be found, in the online version, at <http://dx.doi.org/10.1016/j.jeurceramsoc.2017.09.039>.

## References

- [1] J.J. Spivey, Complete catalytic oxidation of volatile organics, *Ind. Eng. Chem. Res.* 26 (11) (1987) 2165–2180.
- [2] A. Dierstein, H. Natter, F. Meyer, H.-O. Stephan, C. Kropf, R. Hempelmann, Electrochemical deposition under oxidizing conditions (EDOC): a new synthesis for nanocrystalline metal oxides, *Scr. Mater.* 44 (8) (2001) 2209–2212.
- [3] L. Qin, Z. Cheng, M. Guo, J.A. Fan, L.-S. Fan, Morphology evolution and nanostructure of chemical looping transition metal oxide materials upon redox processes, *Acta Mater.* 124 (2017) 568–578.
- [4] D. Wang, Y. Yu, H. He, J. Wang, W. Zhou, H.D. Abruna, Template-free synthesis of hollow-structured  $\text{Co}_3\text{O}_4$  nanoparticles as high-performance anodes for lithium-ion batteries, *ACS Nano* 9 (2) (2015) 1775–1781.
- [5] Z. Lin, W. Yue, D. Huang, J. Hu, X. Zhang, Z.-Y. Yuan, X. Yang, Pore length control of mesoporous  $\text{Co}_3\text{O}_4$  and its influence on the capacity of porous electrodes for lithium-ion batteries, *RSC Adv.* 2 (2012) 1794–1797.
- [6] D. Gu, W. Li, F. Wang, H. Bongard, B. Spleithoff, W. Schmidt, C. Weidenthaler, Y. Xia, D. Zhao, F. Schüth, Controllable synthesis of mesoporous peapod-like  $\text{Co}_3\text{O}_4$ @carbon nanotube arrays for high-performance lithium-ion batteries, *Angew. Chem. Int. Ed.* 54 (24) (2015) 7060–7064.
- [7] X.-H. Xia, J.-P. Tu, Y.-J. Mai, X.-L. Wang, C.-D. Gu, X.-B. Zhao, Self-supported hydrothermal synthesized hollow  $\text{Co}_3\text{O}_4$  nanowire arrays with high supercapacitor capacitance, *J. Mater. Chem.* 21 (25) (2011) 9319–9325.
- [8] D. Kong, C. Cheng, Y. Wang, J.I. Wong, Y. Yang, H.Y. Yang, Three-dimensional  $\text{Co}_3\text{O}_4@\text{C@Ni}_3\text{S}_2$  sandwich-structured nanoneedle arrays: towards high-performance flexible all-solid-state asymmetric supercapacitors, *J. Mater. Chem. A* 3 (2015) 16150–16161.
- [9] J. Yuan, J. Zhu, H. Bi, X. Meng, S. Liang, L. Zhang, X. Wang, Graphene-based 3D composite hydrogel by anchoring  $\text{Co}_3\text{O}_4$  nanoparticles with enhanced electrochemical properties, *Phys. Chem. Chem. Phys.* 15 (31) (2013) 12940–12945.
- [10] Y.-X. Zhang, X. Guo, X. Zhai, Y.-M. Yan, K.-N. Sun, Diethylenetriamine (deta)-assisted anchoring of  $\text{Co}_3\text{O}_4$  nanorods on carbon nanotubes as efficient electrocatalysts for the oxygen evolution reaction, *J. Mater. Chem. A* 3 (2015) 1761–1768.
- [11] A.J. Esswein, M.J. McMurdo, P.N. Ross, A.T. Bell, T.D. Tilley, Size-dependent activity of  $\text{Co}_3\text{O}_4$  nanoparticle anodes for alkaline water electrolysis, *J. Phys. Chem. C* 113 (33) (2009) 15068–15072.
- [12] M. Casas-Cabanas, G. Binotto, D. Larcher, A. Lecup, V. Giordani, J.-M. Tarascon, Defect chemistry and catalytic activity of nanosized  $\text{Co}_3\text{O}_4$ , *Chem. Mater.* 21 (9) (2009) 1939–1947.
- [13] S. Fujita, K. Suzuki, T. Mori, Preparation of high-performance  $\text{Co}_3\text{O}_4$  catalyst for hydrocarbon combustion from co-containing hydrogarnet, *Catal. Lett.* 86 (1–3) (2003) 139–144.
- [14] D.-E. Jiang, S. Dai, The role of low-coordinate oxygen on  $\text{Co}_3\text{O}_4(110)$  in catalytic co-oxidation, *Phys. Chem. Chem. Phys.* 13 (2011) 978–984.
- [15] P. Broqvist, I. Panas, H. Persson, A DFT study on co oxidation over  $\text{Co}_3\text{O}_4$ , *J. Catal.* 210 (1) (2002) 198–206.
- [16] D. Barreca, C. Massignan, S. Daolio, M. Fabrizio, C. Piccirillo, L. Armelao, E. Tondello, Composition and microstructure of cobalt oxide thin films obtained from a novel cobalt (II) precursor by chemical vapor deposition, *Chem. Mater.* 13 (2) (2001) 588–593.
- [17] K. Koumoto, H. Yanagida, Electrical-conduction in pure and Li-substituted  $\text{Co}_3\text{O}_4$ , *J. Am. Ceram. Soc.* 64 (11) (1981) C156–C157.
- [18] A. Kaczmarska, Z. Grzesik, S. Mrowec, On the defect structure and transport properties of  $\text{Co}_3\text{O}_4$  spinel oxide, *High Temp. Mater. Proc.* 31 (2012) 371.
- [19] C.-S. Cheng, M. Serizawa, H. Sakata, T. Hirayama, Electrical conductivity of  $\text{Co}_3\text{O}_4$  films prepared by chemical vapour deposition, *Mater. Chem. Phys.* 53 (3) (1998) 225–230.
- [20] N. Bahlawane, Kinetics of methane combustion over CVD-made cobalt oxide catalysts, *Appl. Catal. B* 67 (3) (2006) 168–176.
- [21] G. Binotto, D. Larcher, A. Prakash, R. Herrera Urbina, M. Hegde, J.-M. Tarascon, Synthesis, characterization, and Li-electrochemical performance of highly porous  $\text{Co}_3\text{O}_4$  powders, *Chem. Mater.* 19 (12) (2007) 3032–3040.
- [22] A. Alivisatos, Naturally aligned nanocrystals, *Science* 289 (5480) (2000) 736–737.
- [23] J.F. Banfield, S.A. Welch, H. Zhang, T.T. Ebert, R.L. Penn, Aggregation-based crystal growth and microstructure development in natural iron oxyhydroxide biominer-alization products, *Science* 289 (5480) (2000) 751–754.
- [24] S. Sakamoto, M. Yoshinaka, K. Hirota, O. Yamaguchi, Fabrication, mechanical properties, and electrical conductivity of  $\text{Co}_3\text{O}_4$  ceramics, *J. Am. Ceram. Soc.* 80 (1) (1997) 267–268.
- [25] M. Hamdani, R. Singh, P. Chartier,  $\text{Co}_3\text{O}_4$  and co-based spinel oxides bifunctional oxygen electrodes, *Int. J. Electrochem. Sci.* 5 (2010) 556–577.
- [26] P. Blöchl, Projector augmented-wave method, *Phys. Rev. B* 50 (24) (1994) 17953.
- [27] G. Kresse, J. Furthmüller, Efficient iterative schemes for ab initio total-energy calculations using a plane-wave basis set, *Phys. Rev. B* 54 (16) (1996) 11169.
- [28] J. Perdew, K. Burke, M. Ernzerhof, Generalized gradient approximation made simple, *Phys. Rev. Lett.* 77 (18) (1996) 3865–3868.
- [29] S. Dudarev, G. Botton, S. Savrasov, C. Humphreys, A. Sutton, Electron-energy-loss spectra and the structural stability of nickel oxide: an LSDA+U study, *Phys. Rev. B* 57 (3) (1998) 1505–1509.
- [30] V.I. Anisimov, J. Zaanen, O.K. Andersen, Band theory and Mott insulators: Hubbard U instead of Stoner I, *Phys. Rev. B* 44 (3) (1991) 943.
- [31] A. Svane, O. Gunnarsson, Transition-metal oxides in the self-interaction-corrected density-functional formalism, *Phys. Rev. Lett.* 65 (1990) 1148–1151.
- [32] J. Chen, X. Wu, A. Selloni, Electronic structure and bonding properties of cobalt oxide in the spinel structure, *Phys. Rev. B* 83 (2011) 245204.
- [33] J. Chen, A. Selloni, Electronic states and magnetic structure at the  $\text{Co}_3\text{O}_4$  (110) surface: a first-principles study, *Phys. Rev. B* 85 (2012) 085306.
- [34] H. Monkhorst, J. Pack, Special points for Brillouin-zone integrations, *Phys. Rev. B* 13 (12) (1976) 5188–5192.
- [35] W. Smith, A. Hobson, The structure of cobalt oxide,  $\text{Co}_3\text{O}_4$ , *Acta Crystallogr. B* 29 (2) (1973) 362–363.
- [36] W. Shaheen, A. Ali, Characterization of solid-solid interactions and physico-chemical properties of copper-cobalt mixed oxides and  $\text{Cu}_x\text{Co}_{3-x}\text{O}_4$  spinels, *Mater. Res. Bull.* 36 (9) (2001) 1703–1716.
- [37] S. Lany, A. Zunger, Accurate prediction of defect properties in density functional supercell calculations, *Modell. Simul. Mater. Sci. Eng.* 17 (8) (2009) 084002.
- [38] J. Ihm, A. Zunger, M.L. Cohen, Momentum-space formalism for the total energy of solids, *J. Phys. C: Solid State Phys.* 12 (21) (1979) 4409.
- [39] G. Makov, M. Payne, Periodic boundary conditions in ab initio calculations, *Phys. Rev. B* 51 (7) (1995) 4014.
- [40] C.G. Van de Walle, J. Neugebauer, First-principles calculations for defects and impurities: applications to III-nitrides, *J. Appl. Phys.* 95 (8) (2004) 3851–3879.
- [41] P. Erhart, K. Albe, A. Klein, First-principles study of intrinsic point defects in  $\text{ZnO}$ : role of band structure, volume relaxation, and finite-size effects, *Phys. Rev. B* 73 (2006) 205203.
- [42] M.W. Chase Jr., NIST-JANAF thermochemical tables, fourth edition, *J. Phys. Chem. Ref. Data, Monogr.* 9 (1998) 1.
- [43] V. Shinde, S. Mahadik, T. Gujar, C. Lokhande, Supercapacitive cobalt oxide ( $\text{Co}_3\text{O}_4$ ) thin films by spray pyrolysis, *Appl. Surf. Sci.* 252 (20) (2006) 7487–7492.
- [44] H. Yamamoto, S. Tanaka, K. Hirao, Nanostructure and optical nonlinearity of cobalt oxide thin films, *J. Ceram. Soc. Jpn.* 112 (2004) S876–S880.
- [45] S. Angelov, E. Zhecheva, R. Stoyanova, M. Atanasov, Bulk defects in  $\text{Co}_3\text{O}_4$ , pure and slightly doped with lithium, revealed by EPR of the tetrahedral  $\text{Co}^{2+}$  ions, *J. Phys. Chem. Solids* 51 (10) (1990) 1157–1161.
- [46] L. Qiao, H.Y. Xiao, H.M. Meyer, J.N. Sun, C.M. Rouleau, A.A. Puretzky, D.B. Geohegan, I.N. Ivanov, M. Yoon, W.J. Weber, M.D. Biegalski, Nature of the band gap and origin of the electro-/photo-activity of  $\text{Co}_3\text{O}_4$ , *J. Mater. Chem. C* 1 (2013) 4628–4633.
- [47] G. Watkins, J. Troxell, Negative-U properties for point defects in silicon, *Phys. Rev. Lett.* 44 (9) (1980) 593.